

Effects of Parasitic Resistances on Magnetically Coupled Impedance-Source Networks

Xiangfei Kong , *Student Member, IEEE*, Chi-Kong Wong , *Member, IEEE*,
and Chi-Seng Lam , *Senior Member, IEEE*

Abstract—Magnetically coupled impedance-source networks can achieve a higher voltage gain with smaller shoot-through duty ratio in comparison with the conventional impedance-source networks without coupled inductors. However, the practical voltage gain is seriously affected by the parasitic resistances in passive components and power devices, which is necessary to be investigated. This article derives and analyzes the effects of parasitic resistances on the voltage gain of magnetically coupled impedance-source networks under three different scenarios: first, different resistance ratio between parasitic resistances and output equivalent resistance, second, different shoot-through duty ratio, and third, different winding ratio. First of all, a generalized equivalent circuit model considering parasitic resistances for the three typical magnetically coupled impedance-source networks—Trans-Z-source, Γ -source, and Y-source networks are proposed. Based on it, the effects of parasitic resistances on the voltage gain is mathematically derived and discussed under the aforementioned three different scenarios. And the maximum voltage gain under the consideration of the three resistance ratios simultaneously is also derived. Finally, representative simulation and experimental results are provided to verify the proposed generalized equivalent circuit models, the corresponding mathematical derivations, and the effects of the parasitic resistances on the magnetically coupled impedance-source networks.

Index Terms—Magnetically coupled impedance-source networks, parasitic resistances, Trans-Z-source, voltage gain, Y-source, Γ -source.

I. INTRODUCTION

IMPEDANCE-SOURCE networks refer to a series of converters suitable for a wide range of power conversion between source and load, including dc/dc, dc/ac, ac/dc, and ac/ac applications. The general block representation of an impedance-source

Manuscript received July 20, 2019; revised October 11, 2019 and December 16, 2019; accepted January 21, 2020. Date of publication January 31, 2020; date of current version May 1, 2020. This work was supported in part by the Science and Technology Development Fund, Macau SAR (FDCT) under Grants 120/2016/A3 and SKL-AMSV Fund and in part by the Research Committee of the University of Macau under Grants MYRG2017-00090-AMSV and MYRG2018-00039-FST. Recommended for publication by Associate Editor Y. Li. (*Corresponding author: Chi-Seng Lam.*)

X. Kong and C.-S. Lam are with the State Key Laboratory of Analog and Mixed-Signal VLSI, University of Macau, Macao 999078, China, with the Institute of Microelectronics, University of Macau, Macao 999078, China, and also with the Department of Electrical and Computer Engineering, Faculty of Science and Technology, University of Macau, Macao 999078, China (e-mail: x.f.kong@connect.um.edu.mo; cslam@um.edu.mo).

C.-K. Wong is with the Department of Electrical and Computer Engineering, Faculty of Science and Technology, University of Macau, Macao 999078, China (e-mail: ckwong@um.edu.mo).

Color versions of one or more of the figures in this article are available online at <https://ieeexplore.ieee.org>.

Digital Object Identifier 10.1109/TPEL.2020.2970831

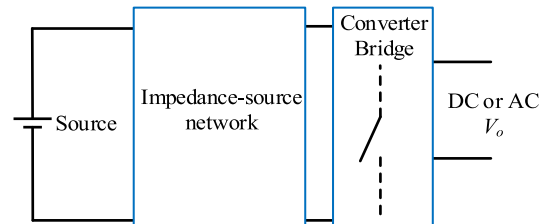


Fig. 1. General block diagram of an impedance-source converter.

converter is shown in Fig. 1, in which the impedance-source network is tied to an input source and a converter bridge implemented with switching devices [1]. Among all the applications, dc/ac conversion with impedance-source networks is most widely used due to proliferation and rapid development of the renewable energy and distribution generation system, etc. In comparison with the conventional voltage source inverters (VSI) which can only achieve buck operation, the impedance-source network supported VSI can achieve the buck-boost operation without additional dc/dc converter stage. As the whole switching cycle of the impedance-source VSI is also composed of shoot-through time besides the modulation time and the ineffective time of the conventional VSI, thus its modulation ratio is less due to the occupation of shoot-through time during a switching cycle.

Z-source network was first proposed in 2002 for both buck and boost capabilities in dc/dc converter applications [2], [3]. After that, switched inductor Z-source [4] and Quasi-Z-source networks [5], were proposed to improve the original Z-source networks, especially on the aspect of voltage gain. Even though a general maximum voltage gain control strategy was proposed to achieve a higher gain of impedance-source networks [6], the voltage gain still cannot be improved significantly because of the limitation of maximum shoot-through duty ratio. To address the insufficient voltage gain problem, magnetically coupled impedance-source network were proposed in [7]–[16] to achieve a higher voltage gain with less shoot-through time. Since the maximum shoot-through time can be determined by the winding ratio of the coupled inductors, the voltage gain characteristic can be changed freely by changing the winding ratio of the coupled inductors [7].

In last decade, different magnetically coupled impedance-source networks have been proposed, such as Trans-Z-source in Fig. 2, Γ -source in Fig. 3, Y-source in Fig. 4, etc. However, nearly all of their voltage gain equations are deduced under ideal

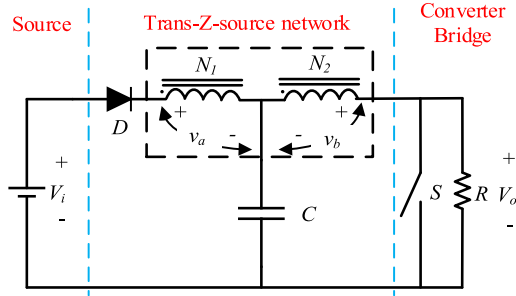


Fig. 2. Trans-Z-source converter.

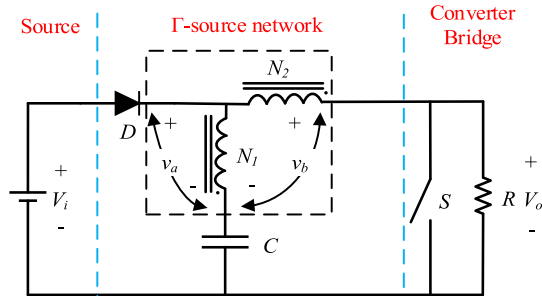
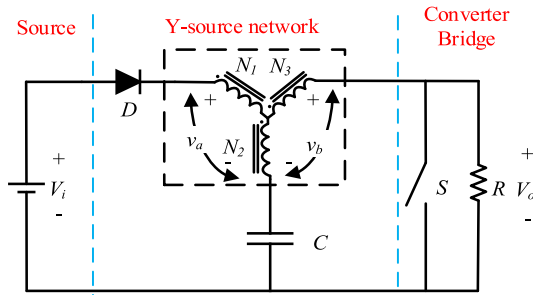
Fig. 3. Γ -source converter.

Fig. 4. Y-source converter.

lossless conditions without considering the network parasitic resistances and leakage inductances. Recently, the effects of leakage inductances on the Y-source network have been gradually paid attention by researchers [17]–[19], which clearly illustrate the leakage inductances strongly affect the output characteristic, and cannot be simply neglected during the design of the impedance-source network. The effects of leakage inductance mainly have two aspects: the voltage spikes when supplying an inductive load and the reduction of voltage gain caused by the reduction of effective shoot-through time. According to the derivation and experimental results in [17], the effective shoot-through time reduces with the increasing of shoot-through duty ratio, which will lead to the reduction of voltage gain. On the other hand, parasitic resistances as another nonignorable factor, are also existed and distributed at all passive components and power devices in practical case, so it is also valuable and necessary to investigate and analyze the effects of parasitic resistances besides leakage inductances. Thus, this article mainly focuses on study and analyze the effects of the parasitic resistances on

the magnetically coupled impedance-source networks. The main contributions of this article are summarized as follows.

- 1) Propose a generalized equivalent circuit models for the three typical magnetically coupled impedance-source networks: Trans-Z-source, Γ -source, and Y-source networks, which simplify their study and analysis with and without parasitic resistances consideration.
- 2) Mathematically derive and analyze the effects of parasitic resistances on the voltage gain of magnetically coupled impedance-source networks under three different conditions: different resistance ratio between parasitic resistances and output equivalent resistance, different shoot-through duty ratio and different winding ratio. And the maximum voltage gain considering all the parasitic resistances simultaneously are also derived.
- 3) Provide different simulation and experimental results to verify the proposed generalized equivalent circuit models, the corresponding mathematical derivations, and the effects of the parasitic resistances on the magnetically coupled impedance-source networks.

The rest of this article is organized as follows. The generalized equivalent circuit model of three different magnetically coupled impedance-source networks is first proposed and discussed in Section II. This is followed by the mathematical derivation of voltage gain in Section III based on the equivalent circuit model. The theoretical study about the effects of parasitic resistances on the voltage gain under different conditions is proposed and discussed in details in Section IV. The correctness of the proposed generalized equivalent circuit models and the corresponding mathematical derivations is verified by representative simulation and experimental results in Section V. Finally, conclusions are drawn in Section VI.

II. EQUIVALENT CIRCUIT MODEL OF DIFFERENT MAGNETICALLY COUPLED IMPEDANCE-SOURCE NETWORKS

Trans-Z-source, Γ -source, and Y-source are three most typical magnetically coupled impedance-source networks. Both Trans-Z-source [8] and Γ -source networks [9], as shown in Figs. 2 and 3, respectively, are composed of two coupled inductors, whereas the Y-source network [10] is composed of three coupled inductors, as shown in Fig. 4. In these figures, V_i and V_o are the input and output voltage; D is a diode; S and R are the equivalent switching device and output equivalent resistance to model as a VSI connected after the impedance source-network; N_1 , N_2 , and N_3 are the windings of the coupled inductors; C is a capacitor.

Although the coupled inductors of these three networks are different, they can ideally achieve the same voltage gain by using different winding ratios [20]. By considering the coupled inductors of these three networks as two-port networks, the winding ratios of the coupled inductors can satisfy the following, provided that the voltages across the windings in Figs. 2–4 follow the criteria in (2), (3), and (4), respectively:

$$v_a : v_b = N_a : N_b \quad (1)$$

where v_a and v_b are the voltages of the two-port networks, N_a and N_b are the equivalent winding numbers of the two-port network.

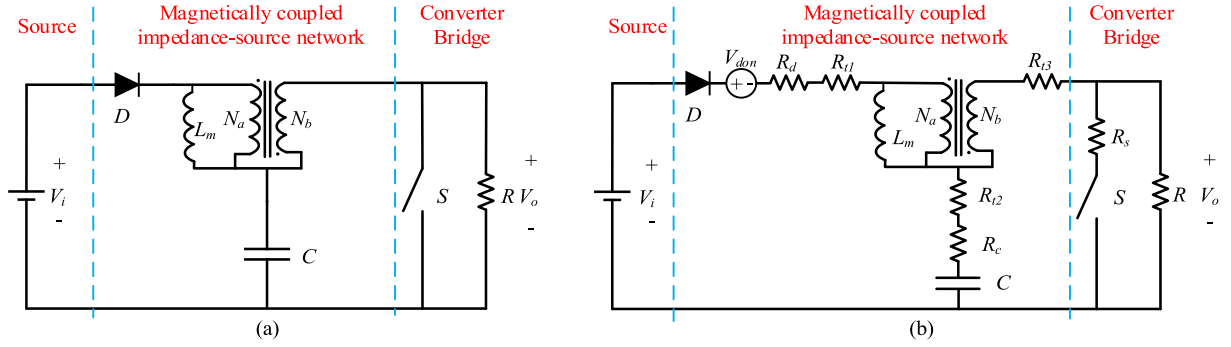


Fig. 5. Equivalent circuit models of magnetically coupled impedance-source converter under: (a) ideal lossless condition and (b) parasitic resistances condition.

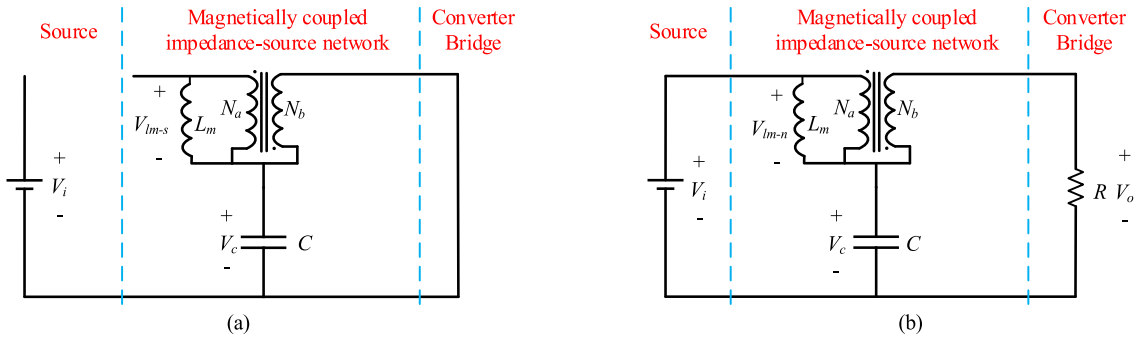


Fig. 6. Equivalent circuit models under ideal lossless condition during: (a) shoot-through state and (b) nonshoot-through state.

Trans-Z-source satisfies

$$(2) \quad \begin{cases} N_1 = N_a \\ N_2 = N_b. \end{cases}$$

Γ -source satisfies

$$(3) \quad \begin{cases} N_1 = N_a \\ N_2 = N_a + N_b. \end{cases}$$

Y-source satisfies

$$(4) \quad \begin{cases} N_1 + N_2 = N_a \\ N_3 - N_2 = N_b. \end{cases}$$

Based on the above analysis, the generalized equivalent circuit model for the Trans-Z-source, Γ -source, and Y-source under ideal lossless condition is shown in Fig. 5(a), where L_m is the equivalent magnetic inductance of the primary side, and N_a : N_b is the winding ratio of the ideal coupled inductors. Furthermore, Fig. 5(b) shows the generalized equivalent circuit model under parasitic resistances consideration, in which the diode D is modeled as a voltage drop and a resistor during the switching-ON period, whereas the switching device S is modeled as a resistor during the switching-ON period. In addition, the coupled inductors have winding resistances, whereas the capacitor has equivalent series resistance (ESR). In Fig. 5(b), R_{t1} , R_{t2} , and R_{t3} are the winding resistances of coupled inductors, V_{don} is the voltage drop of the diode, R_c , R_d , and R_s are the parasitic resistances of the capacitor, diode, and switching device, respectively.

III. MATHEMATICAL DERIVATION OF VOLTAGE GAIN

A. Under Ideal Lossless Condition

From Fig. 5(a), the voltage gain of the magnetically coupled impedance-source converter under ideal lossless condition can be derived. Shoot-through state happens when the switching device S is turned ON as shown in Fig. 6(a), whereas the nonshoot-through state happens when the switching device S is turned OFF as shown in Fig. 6(b). In Fig. 6, V_{lm-s} and V_{lm-n} are the voltage of magnetic inductor during shoot-through and nonshoot-through states, V_c is the voltage of the capacitor.

During the shoot-through state as in Fig. 6(a), according to Kirchhoff's Voltage Law (KVL), it yields

$$(5) \quad V_c - V_{lm-s} \frac{N_b}{N_a} = 0.$$

Similarly, during the nonshoot-through state as shown in Fig. 6(b), it yields

$$(6) \quad V_c + V_{lm-n} = V_i.$$

Following the voltage-second balance principle (LVSB) of the magnetic inductor, the magnetic inductor voltage of the two states should satisfy

$$(7) \quad D_{st} V_{lm-s} + (1 - D_{st}) V_{lm-n} = 0$$

where D_{st} is the shoot-through duty ratio.

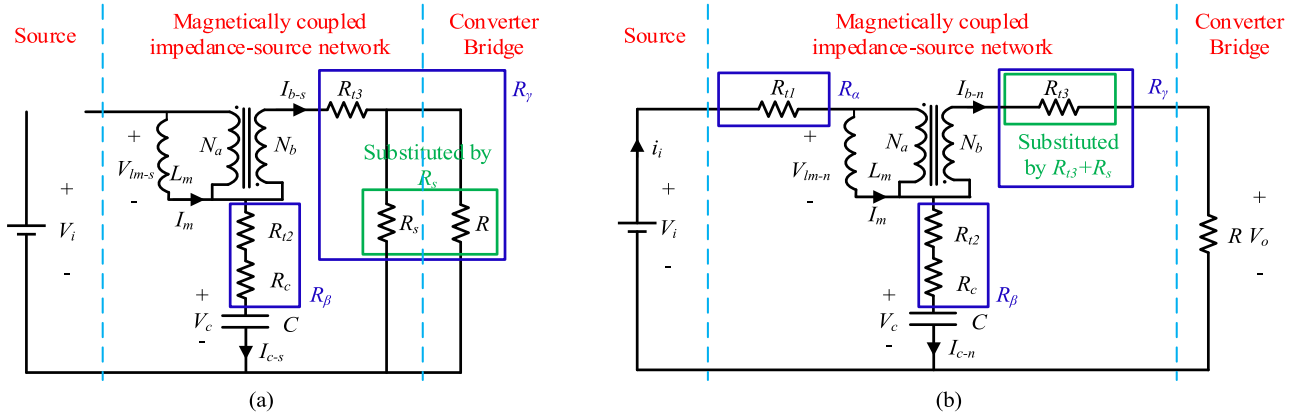


Fig. 7. Equivalent circuit models under parasitic resistances condition during: (a) shoot-through state and (b) nonshoot-through state.

Based on (5)–(7), the voltage of the capacitor can be derived as

$$V_c = \frac{1 - D_{st}}{1 - \frac{N_a + N_b}{N_b} D_{st}} V_i. \quad (8)$$

According to KVL, the capacitor voltage can be rewritten as

$$V_c - \frac{N_b}{N_a} V_{lm-n} = V_o. \quad (9)$$

Based on (6)–(9), the output voltage can be derived, then the voltage gain can be derived as

$$\frac{V_o}{V_i} = \frac{1}{1 - (1 + K) D_{st}} \quad (10)$$

where $K = N_a : N_b$.

B. Under Parasitic Resistances Condition

From Fig. 5(b), the voltage gain of the magnetically coupled impedance-source converter under parasitic resistances condition can be derived. When the controlled switching device S is turned on or turned OFF, the equivalent circuit models of the shoot-through and nonshoot-through states are shown in Fig. 7(a) and (b), respectively. Since the VSI is usually connected after the impedance-source network for the power grid dc/ac inversion, the output equivalent resistance of the impedance-source converter will be much larger than the ON-resistance of the switching devices. Therefore, during shoot-through state as shown in Fig. 7(a), the ON-resistance of the switching device R_s and output equivalent resistance R can be simplified as the on-resistance of the switching devices R_s . And $R_{t2} + R_c$ is expressed as R_β , whereas $R_{t3} + R_s$ is expressed as R_γ in this article. During the nonshoot-through state as shown in Fig. 7(b), in order to simplify the analysis (consistent with the shoot-through state: $R_\gamma = R_{t3} + R_s$), the winding resistance R_{t3} can be substituted by $R_{t3} + R_s$, and then expressed as R_γ . As R_s is much smaller than the output equivalent resistance R , the effect of R_s to the output can be neglected. The diode is conducted during nonshoot-through state, since the voltage drop of diode V_{don} is much smaller than the input voltage while the resistance of diode R_d is also much smaller than the resistances

of windings, capacitor and switching device, the effects of diode on the voltage gain can be neglected for simplification. Then, R_{t1} is expressed as R_α in this article. Besides, from Fig. 7, i_{b-s} and i_{b-n} are the currents of the secondary winding during shoot-through and nonshoot-through states; i_{c-s} and i_{c-n} are the currents of capacitor during shoot-through and nonshoot-through states; i_i is the input current; I_m is the magnetic current. When the magnetic inductance is large enough, I_m can be regarded as a fixed value during shoot-through and nonshoot-through stages for simplicity.

During shoot-through state as shown in Fig. 7(a), according to KVL, it yields

$$V_c - \frac{N_b}{N_a} V_{lm-s} - i_{b-s}(R_\beta + R_\gamma) = 0. \quad (11)$$

The current of the secondary winding during shoot-through state can be expressed as

$$i_{b-s} = \frac{N_a}{N_b} I_m. \quad (12)$$

Based on Kirchoff's current law (KCL), the current of the capacitor during shoot-through state can be expressed as

$$i_{c-s} = -i_{b-s}. \quad (13)$$

During the nonshoot-through state as shown in Fig. 7(b), based on KVL, it yields

$$V_i - i_i R_\alpha - V_{lm-n} - V_c - i_{c-n} R_\beta = 0 \quad (14)$$

$$V_c - \frac{N_b}{N_a} V_{lm-n} - V_o + i_{c-n} R_\beta - i_{b-n} R_\gamma = 0. \quad (15)$$

The current of the secondary winding during nonshoot-through state can be expressed as

$$i_{b-n} = \frac{N_a}{N_b} (I_m - i_i). \quad (16)$$

Based on KCL, it yields

$$i_{c-n} + i_{b-n} = i_i. \quad (17)$$

Considering both shoot-through and nonshoot-through states, based on LVSB of the magnetic inductor, the magnetic inductor

voltage of the two states should satisfy

$$D_{st}V_{lm-s} + (1 - D_{st})V_{lm-n} = 0. \quad (18)$$

Following the ampere second balance (CASB) principle of the capacitor, the capacitor current of the two states should satisfy

$$D_{st}i_{c-s} + (1 - D_{st})i_{c-n} = 0. \quad (19)$$

And the output equivalent resistance can be expressed as

$$R = \frac{V}{i_{b-n}}. \quad (20)$$

Based on (11)–(20), the voltage gain under parasitic resistances condition can be derived as

$$\frac{V_o}{V_i} = \frac{1}{f + f_\alpha\alpha + f_\beta\beta + f_\gamma\gamma} \quad (21)$$

where $\alpha = R_\alpha/R$, $\beta = R_\beta/R$, $\gamma = R_\gamma/R$ are the three different parasitic resistance ratios α , β , and γ with respect to output equivalent resistance. f , f_α , f_β , and f_γ are the voltage gain influence factors due to the ideal lossless condition and the three different parasitic resistance ratios α , β , and γ , respectively, which can be expressed as

$$f = 1 - (1 + K)D_{st} \quad (22)$$

$$f_\alpha = \frac{1}{1 - (1 + K)D_{st}} \quad (23)$$

$$f_\beta = \frac{(1 + K)^2 D_{st}}{1 - (1 + K)D_{st}} \quad (24)$$

$$f_\gamma = \frac{1 - D_{st} + K^2 D_{st}}{1 - (1 + K)D_{st}}. \quad (25)$$

IV. EFFECTS OF PARASITIC RESISTANCES ON VOLTAGE GAIN

Under ideal lossless condition, the voltage gain in (10) is only related to the winding ratio and shoot-through duty ratio. However, when the parasitic resistances are taken into consideration, the voltage gain in (21) is related to the effects of parasitic resistances ratios represented by α , β , and γ , and also the winding ratio and shoot-through duty ratio. In the following, the effects of the parasitic resistances on the voltage gain of the magnetically coupled impedance-source converter under three different conditions: different resistance ratios between parasitic resistances and output equivalent resistance, different shoot-through duty ratio, and different winding ratio will be studied and investigated in details. Besides, the maximum voltage gain considering all the parasitic resistances simultaneously is also derived.

A. Resistance Ratio

The voltage gain is affected by three different parasitic resistance ratios α , β , and γ .

1) *Under Ideal Lossless Condition*: When the parasitic resistances are not taken into consideration, only f exists in (21), thus the voltage gain in (21) can be rewritten as

$$\frac{V_o}{V_i} \Big|_{\alpha=0, \beta=0, \gamma=0} = \frac{1}{1 - (1 + K)D_{st}}. \quad (26)$$

By comparing (10) with (26), the voltage gain under ideal lossless condition is a special case of (21) when only the factor f is valid without considering parasitic resistances.

When the parasitic resistances are taken into consideration individually to investigate their different effects on the output, the voltage gains can be expressed as the following equations:

2) *Ratio α* :

$$\frac{V_o}{V_i} \Big|_{\beta=0, \gamma=0} = \frac{1}{1 - (1 + K)D_{st} + \frac{1}{1 - (1 + K)D_{st}}\alpha}. \quad (27)$$

3) *Ratio β* :

$$\frac{V_o}{V_i} \Big|_{\alpha=0, \gamma=0} = \frac{1}{1 - (1 + K)D_{st} + \frac{(1 + K)^2 D_{st}}{1 - (1 + K)D_{st}}\beta}. \quad (28)$$

4) *Ratio γ* :

$$\frac{V_o}{V_i} \Big|_{\alpha=0, \beta=0} = \frac{1}{1 - (1 + K)D_{st} + \frac{1 - D_{st} + K^2 D_{st}}{1 - (1 + K)D_{st}}\gamma}. \quad (29)$$

For all the cases, the voltage gain is affected by the ratios of the parasitic resistances and output equivalent resistance that are α , β , and γ , rather than the single parasitic resistance. From (27)–(29), the voltage gain is affected more seriously with the increasing of resistance ratios α , β , and γ .

B. Shoot-Through Duty Ratio

1) *Under Ideal Lossless Condition*: From (21), the shoot-through duty ratio D_{st} can also affect the voltage gain of the magnetically coupled impedance-source converter. Under ideal lossless condition, the monotonicity of voltage gain function can be analyzed by the polarity of differential function. The partial differential function of (26) can be solved as

$$\frac{\partial V_o}{\partial D_{st}} \Big|_{\alpha=0, \beta=0, \gamma=0} = \frac{1 + K}{[1 - (1 + K)D_{st}]^2}. \quad (30)$$

Since the numerator and denominator of (30) are both positive, the partial differential function is always larger than 0, which means that the voltage gain increases with the increasing of D_{st} .

2) *Ratio α* : When the ratio α is considered, the partial differential function of (27) can be solved as

$$\frac{\partial V_o}{\partial D_{st}} \Big|_{\beta=0, \gamma=0} = \frac{(1 + K)}{(f + f_\alpha\alpha)^2} \left\{ 1 - \frac{\alpha}{[1 - (1 + K)D_{st}]^2} \right\}. \quad (31)$$

As

$$\frac{(1 + K)}{(f + f_\alpha\alpha)^2} > 0 \quad (32)$$

the polarity of (31) is larger than 0 when it satisfies

$$1 - \frac{\alpha}{[1 - (1 + K)D_{st}]^2} \geq 0. \quad (33)$$

Solving (33) yields,

$$0 < D_{st} \leq \frac{1 - \sqrt{\alpha}}{1 + K}. \quad (34)$$

On the contrary, when

$$1 - \frac{\alpha}{[1 - (1 + K)D_{st}]^2} < 0. \quad (35)$$

Solving (35) yields

$$D_{st} > \frac{1 - \sqrt{\alpha}}{1 + K}. \quad (36)$$

Based on (31)–(36), it can be seen that (27) is an increasing function, when D_{st} satisfies (34). After the voltage gain reaches a peak value, it is a decreasing function, when the D_{st} satisfies (36). In other words, when α is considered, the voltage gain increases and then decreases after reaching the peak value, and the maximum point is at

$$D_{st} = \frac{1 - \sqrt{\alpha}}{1 + K} \quad (37)$$

and the maximum voltage gain can be solved as

$$\frac{V_o}{V_i} \Big|_{\beta=0, \gamma=0, D_{st}=\frac{1-\sqrt{\alpha}}{1+K}} = \frac{1}{2\sqrt{\alpha}}. \quad (38)$$

3) *Ratio β* : When the ratio β is considered, the partial differential function of (28) can be solved as

$$\frac{\partial V_o}{\partial D_{st}} \Big|_{\alpha=0, \gamma=0} = \frac{(1 + K)}{(f + f_\beta \beta)^2} \left\{ 1 - \frac{(1 + K)\beta}{[1 - (1 + K)D_{st}]^2} \right\}. \quad (39)$$

Following the same deduction approach as the ratio α , the polarity of (39) can be determined as

$$1 - \frac{(1 + K)\beta}{[1 - (1 + K)D_{st}]^2} \begin{cases} \geq 0, 0 < D_{st} \leq \frac{1 - \sqrt{(1 + K)\beta}}{1 + K} \\ < 0, \frac{1 - \sqrt{(1 + K)\beta}}{1 + K} < D_{st} < \frac{1}{1 + K}. \end{cases} \quad (40)$$

Based on (39) and (40), when β is the considered resistance ratio, the voltage gain increases, and then decreases after reaching a peak value, and the maximum point is at

$$D_{st} = \frac{1 - \sqrt{(1 + K)\beta}}{1 + K} \quad (41)$$

and the maximum voltage gain can be solved as

$$\frac{V_o}{V_i} \Big|_{\alpha=0, \gamma=0, D_{st}=\frac{1-\sqrt{(1+K)\beta}}{1+K}} = \frac{1}{1 - (1 - \sqrt{(1 + K)\beta})^2}. \quad (42)$$

4) *Ratio γ* : When the ratio γ is considered, the partial differential function of (29) can be solved as

$$\frac{\partial V_o}{\partial D_{st}} \Big|_{\alpha=0, \beta=0} = \frac{(1 + K)}{(f + f_\gamma \gamma)^2} \left[1 - \frac{K\gamma}{[1 - (1 + K)D_{st}]^2} \right]. \quad (43)$$

Following the same deduction approach as the ratio α and β , the polarity of (43) can be determined as

$$1 - \frac{K\gamma}{[1 - (1 + K)D_{st}]^2} \begin{cases} \geq 0, 0 < D_{st} \leq \frac{1 - \sqrt{K\gamma}}{1 + K} \\ < 0, \frac{1 - \sqrt{K\gamma}}{1 + K} < D_{st} < \frac{1}{1 + K}. \end{cases} \quad (44)$$

Based on (43) and (44), when γ is the considered factor, the voltage gain increases first and then decreases after reaching a peak value, and the maximum point is at

$$D_{st} = \frac{1 - \sqrt{K\gamma}}{1 + K} \quad (45)$$

and the maximum voltage gain can be solved as

$$\frac{V_o}{V_i} \Big|_{\alpha=0, \beta=0, D_{st}=\frac{1-\sqrt{K\gamma}}{1+K}} = \frac{1}{-(1 - \sqrt{K\gamma})^2 + \gamma + 1}. \quad (46)$$

C. Winding Ratio

1) *Under Ideal Lossless Condition*: From (21), the winding ratio K can also affect the voltage gain of the magnetically coupled impedance-source converter. Under ideal lossless condition, the maximum voltage gain in (26) can achieve ∞ under any winding ratios when D_{st} is close to $1/(1+K)$.

2) *Ratio α* : When the ratio α is considered, based on the maximum voltage gain function (38), it has nothing to do with K , which means that the maximum voltage gain will be a fixed value under different winding ratios of the coupled inductors.

3) *Ratio β* : When the ratio β is considered, based on the maximum voltage gain function (42), it is a decreasing function of K . Therefore, the maximum voltage gain will decrease when the winding ratio of the coupled inductors increases.

4) *Ratio γ* : When the ratio γ is considered, based on the maximum voltage gain function (46), it is also a decreasing function of K . Therefore, the maximum voltage gain will decrease with the increasing of winding ratio.

D. Voltage Gain Curves Under Parasitic Resistances Condition

The voltage gain curves under parasitic resistances condition are shown in Fig. 8 when the resistance ratio: (a) α , (b) β , and (c) γ is considered, respectively, under different shoot-through duty ratio D_{st} and different winding ratio K values.

The voltage gain will be infinite under ideal lossless condition which has been discussed among the existing literatures [8]–[10]. From Fig. 8, the voltage gain will be significantly limited with the increasing of resistance ratio α , β , and γ , which is consistent with the derivations in Section IV part A.

From Fig. 8, for all resistance ratio α , β , and γ cases, the voltage gain increases with the increasing of shoot-through duty ratio first, and then decreases after reaching a peak value, which is consistent with the derivations in Section IV part B.

From Fig. 8(a), the maximum voltage gain keeps at a constant value with different winding ratios. From Fig. 8(b) and (c), the maximum voltage gain are significantly affected with the increasing of winding ratios, which is consistent with the derivations in Section IV part C.

E. Maximum Voltage Gain Under Ratios α , β , and γ Consideration

Based on the above analysis, the voltage gain is affected by parasitic resistances in comparison with ideal lossless case, in which the effects on voltage gain under resistance ratios α , β ,

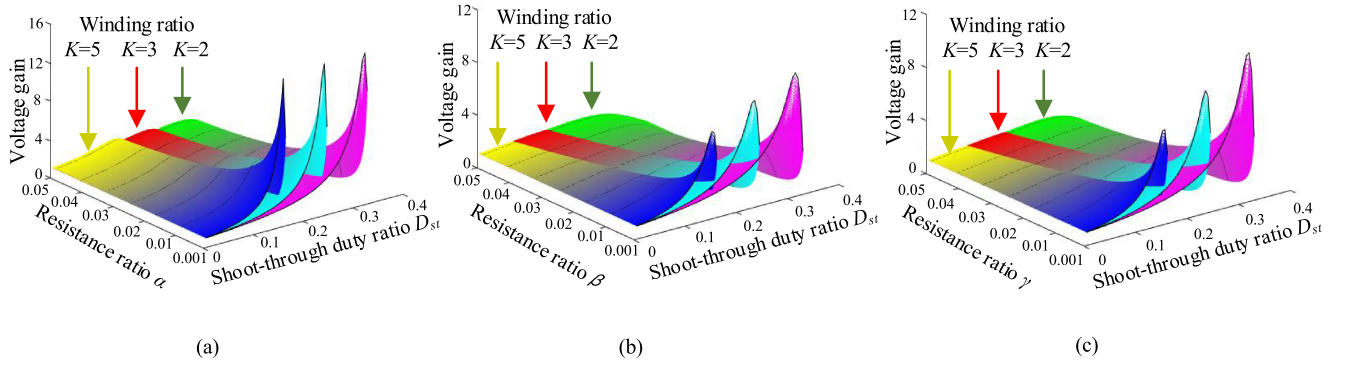


Fig. 8. Voltage gain under parasitic resistances condition when the resistance ratio: (a) α , (b) β , and (c) γ are considered under different D_{st} and K values.

and γ are derived and analyzed separately, so as to investigate the effects of each ratio. However, none of these three ratios is zero in practical case, thus it is more practical and valuable to deduce the maximum voltage gain, when α , β , and γ are considered simultaneously.

From the voltage gain under ratios α , β , and γ consideration in (21), its partial differential function can be derived as

$$\frac{\partial V_o}{\partial D_{st}} = \frac{(1+K)}{(f+f_\alpha\alpha+f_\beta\beta+f_\gamma\gamma)^2} \times \left\{ 1 - \frac{\alpha + (1+K)\beta + K\gamma}{[1 - (1+K)D_{st}]^2} \right\}. \quad (47)$$

Following the same analysis method as for the ratio α , β , and γ cases, the voltage gain increases first with the increasing of D_{st} , and then decrease after reaching a peak value, the D_{st} at the maximum point can be solved as

$$D_{st} = \frac{1 - \sqrt{\alpha + (1+K)\beta + K\gamma}}{1+K}. \quad (48)$$

Then, by substituting (48) into (21), the maximum voltage gain under ratios α , β , and γ consideration can be solved as

$$\frac{V_o}{V_i} \Big|_{D_{st} = \frac{1 - \sqrt{\alpha + (1+K)\beta + K\gamma}}{1+K}} = \frac{1}{2\sqrt{\alpha + (1+K)\beta + K\gamma} - (1+K)\beta + (1-K)\gamma}. \quad (49)$$

V. SIMULATION AND EXPERIMENTAL RESULTS

A. Simulation Verification

The simulation studies have been done by using Matlab to verify the correctness of the proposed generalized equivalent circuit models and the corresponding mathematical derivations in this article. The parasitic resistance ratio α is simulated by R_α divided by the output equivalent resistance R . The parasitic resistance ratio β is simulated by R_β divided by R . The parasitic resistance ratio γ is simulated by R_γ divided by R , and the general simulation parameters are shown in Table I.

TABLE I

GENERAL SIMULATION PARAMETERS OF EQUIVALENT CIRCUIT MODEL

Input voltage V_i	20V
Switching frequency	20kHz
Magnetic inductance L_m	1mH
Capacitance C	330 μ F
Output equivalent resistance R	50 Ω & 100 Ω

TABLE II

SIMULATION PARAMETERS TO VERIFY EQUIVALENT CIRCUIT MODEL

	TRANS-Z-SOURCE (EQUIVALENT CIRCUIT)		
	Γ -SOURCE	Y-SOURCE	
Winding number K	3:1	3:4	2:1:2
Magnetic inductance L_m	1mH	1mH	0.667mH

1) Verification of Generalized Equivalent Circuit Models:

To verify the generalized equivalent circuit models, the corresponding simulation parameters are shown in Table II to achieve the same voltage gain theoretically based on the analysis in Section II. The simulation results under both ideal lossless and parasitic resistance conditions are shown in Fig. 9. It can be seen that all the three topologies of magnetically coupled impedance-source converters can achieve the same voltage gain under both ideal lossless and parasitic resistance conditions. Fig. 9 verifies that the generalized equivalent circuit model can represent these three typical magnetically coupled impedance-source converters.

2) Resistance Ratio:

To verify the effects of parasitic resistances or parasitic resistance ratios α , β , and γ on the voltage gain and the derived theoretical equations, the corresponding simulation results are shown in Fig. 10. In Fig. 10(a) and (d), their simulated output voltages V_o are both less than the ideal lossless case due to the parasitic resistance R_α , and the simulated V_o values are consistent with the theoretical values. Although the parasitic resistance R_α of Fig. 10(a) and (d) are the same, the voltage gain of Fig. 10(d) is affected more seriously than that

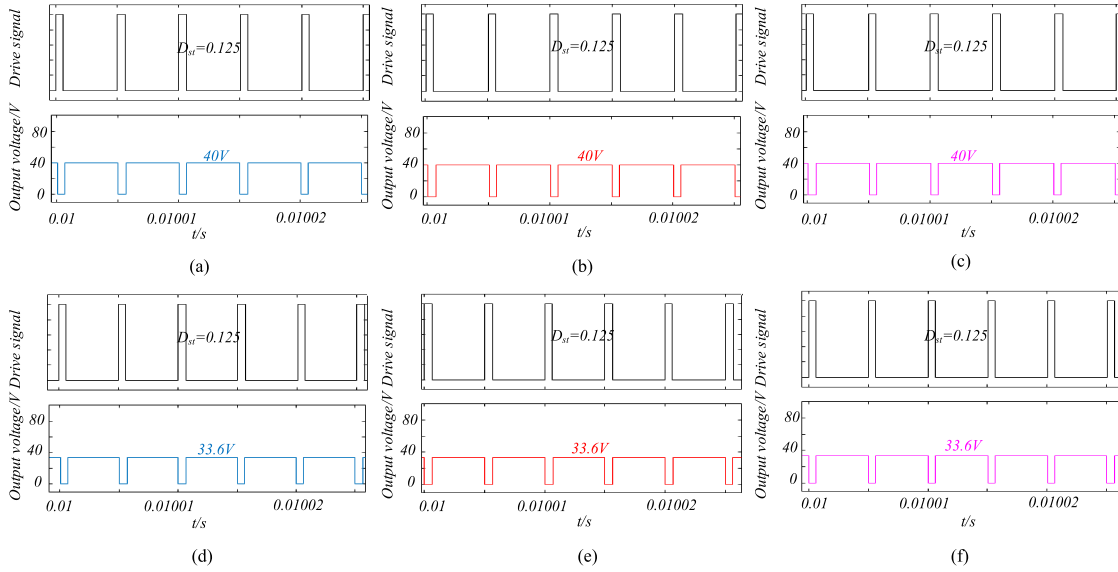


Fig. 9. Simulation results of generalized equivalent circuit models. (a) Trans-Z-source (equivalent circuit) under ideal lossless condition. (b) Γ -source under ideal lossless condition. (c) Y-source under ideal lossless condition. (d) Trans-Z-source (equivalent circuit) under parasitic resistances condition: $R_\alpha = 0.5\Omega$, $R_\beta = 0.5\Omega$, $R_\gamma = 0.5\Omega$, $R = 50\Omega$ ($\alpha = 0.01$, $\beta = 0.01$, $\gamma = 0.01$). (e) Γ -source under parasitic resistances condition: $R_\alpha = 0.5\Omega$, $R_\beta = 0.5\Omega$, $R_\gamma = 0.5\Omega$, $R = 50\Omega$ ($\alpha = 0.01$, $\beta = 0.01$, $\gamma = 0.01$). (f) Y-source under parasitic resistances condition: $R_\alpha = 0.5\Omega$, $R_\beta = 0.5\Omega$, $R_\gamma = 0.5\Omega$, $R = 50\Omega$ ($\alpha = 0.01$, $\beta = 0.01$, $\gamma = 0.01$).

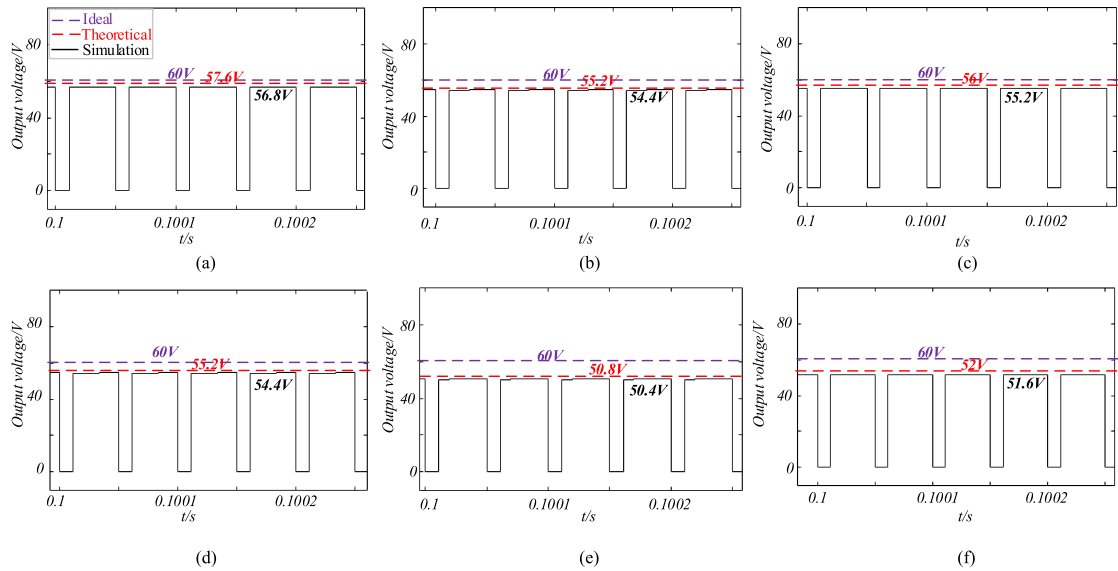


Fig. 10. Simulation results of V_o versus resistance ratios α , β , and γ under $K = 2:1$ and $D_{st} = 0.22$. (a) $R_\alpha = 0.5\Omega$, $R_\beta = 0$, $R_\gamma = 0$, $R = 100\Omega$ ($\alpha = 0.005$, $\beta = 0$, $\gamma = 0$). (b) $R_\alpha = 0$, $R_\beta = 0.5\Omega$, $R_\gamma = 0$, $R = 100\Omega$ ($\alpha = 0$, $\beta = 0.005$, $\gamma = 0$). (c) $R_\alpha = 0$, $R_\beta = 0$, $R_\gamma = 0.5\Omega$, $R = 100\Omega$ ($\alpha = 0$, $\beta = 0$, $\gamma = 0.005$). (d) $R_\alpha = 0.5\Omega$, $R_\beta = 0$, $R_\gamma = 0$, $R = 50\Omega$ ($\alpha = 0.01$, $\beta = 0$, $\gamma = 0$). (e) $R_\alpha = 0$, $R_\beta = 0.5\Omega$, $R_\gamma = 0$, $R = 50\Omega$ ($\alpha = 0$, $\beta = 0.01$, $\gamma = 0$). (f) $R_\alpha = 0$, $R_\beta = 0$, $R_\gamma = 0.5\Omega$, $R = 50\Omega$ ($\alpha = 0$, $\beta = 0$, $\gamma = 0.01$).

of Fig. 10(a) due to a higher α . The same conclusions can be drawn when comparing Fig. 10(b) with Fig. 10(e), and (c) with Fig. 10(f). Fig. 10 clearly illustrates that the voltage gain is significantly affected by the ratio between the parasitic resistance and equivalent output resistance, but not only the parasitic resistance. And the voltage gain is affected more seriously due to a higher resistance ratio. According to the simulation results in Fig. 10, the correctness of the mathematical derivations and analysis of the voltage gain of the magnetically coupled impedance-source converter under parasitic resistance conditions in Section IV part A can be verified.

3) *Shoot-Through Duty Ratio*: To verify the effects of shoot-through duty ratio D_{st} on the voltage gain under parasitic resistance ratios α , β , and γ conditions and the derived theoretical equations, the corresponding simulation results are shown in Fig. 11 with the shoot-through duty ratio D_{st} changes from 0.22 to 0.32. The theoretical V_o curves are plotted based on (27), (28) and (29) and the maximum points are determined by (37), (38), (41), (42), (45), and (46). From Fig. 11, the V_o or voltage gain increases first and then decreases after reaching a peak value when the resistance ratio α , β , and γ is considered, respectively. And the simulated maximum V_o values and the maximum points

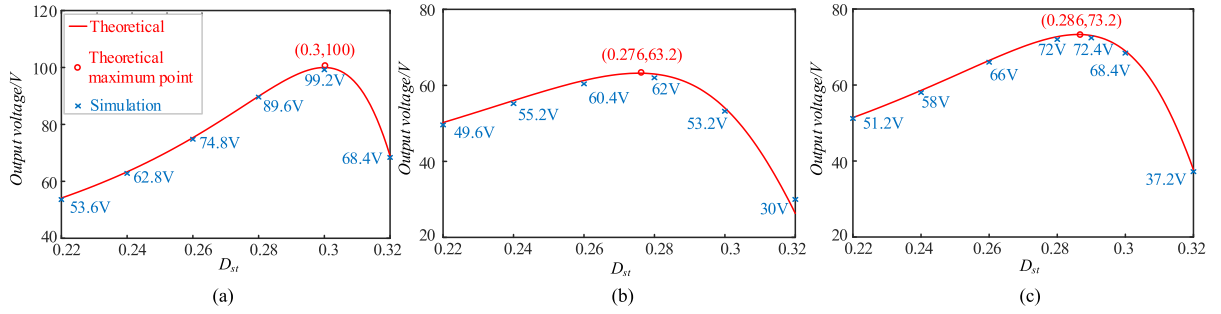


Fig. 11. Simulation results of V_o versus shoot-through duty ratio D_{st} under $K = 2:1$, $R = 50 \Omega$. (a) $R_\alpha = 0.5 \Omega$, $R_\beta = 0$, $R_\gamma = 0$ ($\alpha = 0.01$, $\beta = 0$, $\gamma = 0$). (b) $R_\alpha = 0$, $R_\beta = 0.5 \Omega$, $R_\gamma = 0$ ($\alpha = 0$, $\beta = 0.01$, $\gamma = 0$). (c) $R_\alpha = 0$, $R_\beta = 0$, $R_\gamma = 0.5 \Omega$ ($\alpha = 0$, $\beta = 0$, $\gamma = 0.01$).

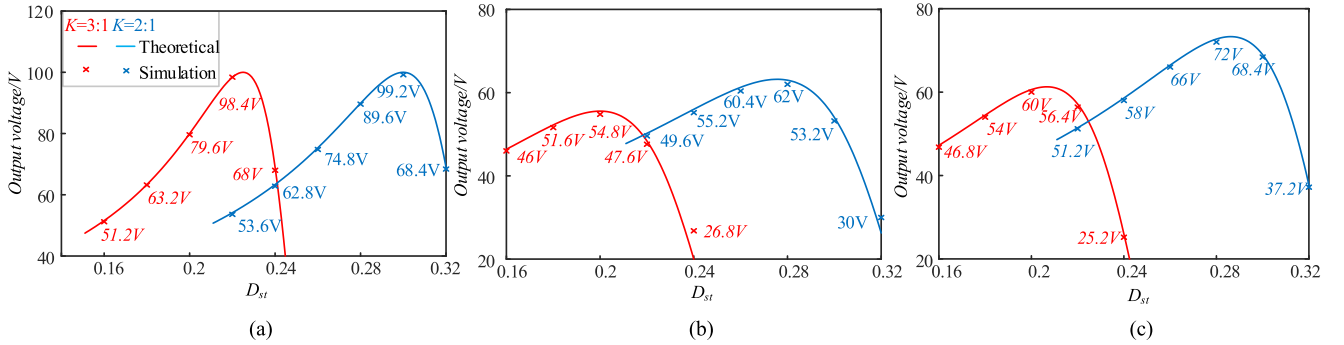


Fig. 12. Simulation results of V_o versus winding ratio K under $R = 50 \Omega$. (a) $R_\alpha = 0.5 \Omega$, $R_\beta = 0$, $R_\gamma = 0$ ($\alpha = 0.01$, $\beta = 0$, $\gamma = 0$). (b) $R_\alpha = 0$, $R_\beta = 0.5 \Omega$, $R_\gamma = 0$ ($\alpha = 0$, $\beta = 0.01$, $\gamma = 0$). (c) $R_\alpha = 0$, $R_\beta = 0$, $R_\gamma = 0.5 \Omega$ ($\alpha = 0$, $\beta = 0$, $\gamma = 0.01$).

TABLE III
PARAMETERS OF EXPERIMENTAL PROTOTYPE

Input voltage V_i	20V	
Switching frequency	20kHz	
Diode D	FFSP1065A	
Switch device S	SCT3022ALGC11, $R_s=0.022\Omega$	
Capacitors C	EPCOS B43501-AS5337-M, 330 μ F, 450V, $R_{ESR}=0.2\Omega$ at 20kHz 20–60 $^\circ$ C	
Magnetic core	Ferrite EE55B with air gaps	
Coils	Multiple stranded copper wire, $\Phi 0.1\text{mm} \times 100$, 0.0022 Ω / 1 turn	
Output equivalent resistance R	50 Ω	
Trans-Z-source ($N_1:N_2=36:18$)	R_α (α)	0.0792 Ω (0.0016)
	R_β (β)	0.2 Ω (0.0040)
	R_γ (γ)	0.0616 Ω (0.0012)
Trans-Z-source ($N_1:N_2=36:12$)	R_α (α)	0.0792 Ω (0.0016)
	R_β (β)	0.2 Ω (0.0040)
	R_γ (γ)	0.0484 Ω (0.0010)
Γ -source ($N_1:N_2=36:48$)	R_α (α)	0 Ω (0)
	R_β (β)	0.2792 Ω (0.0056)
	R_γ (γ)	0.1276 Ω (0.0026)
Y-source ($N_1:N_2:N_3=30:6:18$)	R_α (α)	0.0660 Ω (0.0013)
	R_β (β)	0.2132 Ω (0.0043)
	R_γ (γ)	0.0616 Ω (0.0012)

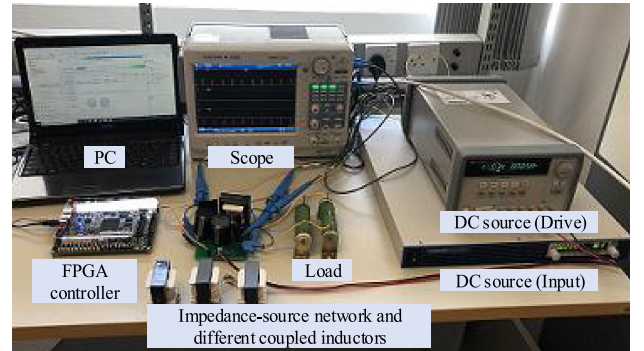


Fig. 13. Experimental prototype of the magnetically coupled impedance-source converter.

are also consistent with the theoretical values. According to the simulation results in Fig. 11, the mathematical derivations and analysis in Section IV part B can be verified.

4) *Winding Ratio*: To verify the effects of winding ratio K on the voltage gain under parasitic resistance ratios α , β , and γ conditions and the derived theoretical equations, the corresponding simulation results are shown in Fig. 12. From Fig. 12(a), the maximum V_o or voltage gain keeps approximately constant with different winding ratios when only ratio α is considered. From Fig. 12(b) and (c), the maximum V_o or voltage gains are significantly affected with the increasing of winding ratios, when only β or γ is considered. According to the simulation results in

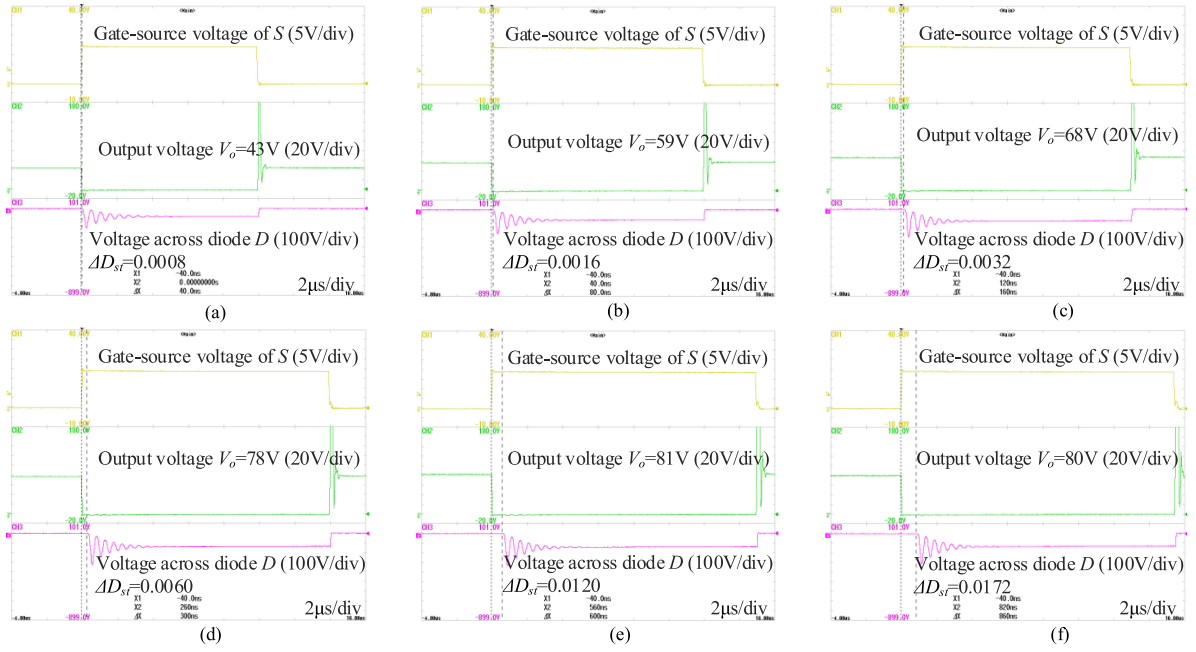


Fig. 14. Experimental results of Trans-Z-source with $N_1:N_2 = 36:18$. (a) $D_{st} = 0.20$. (b) $D_{st} = 0.24$. (c) $D_{st} = 0.26$. (d) $D_{st} = 0.28$. (e) $D_{st} = 0.30$. (f) $D_{st} = 0.31$.

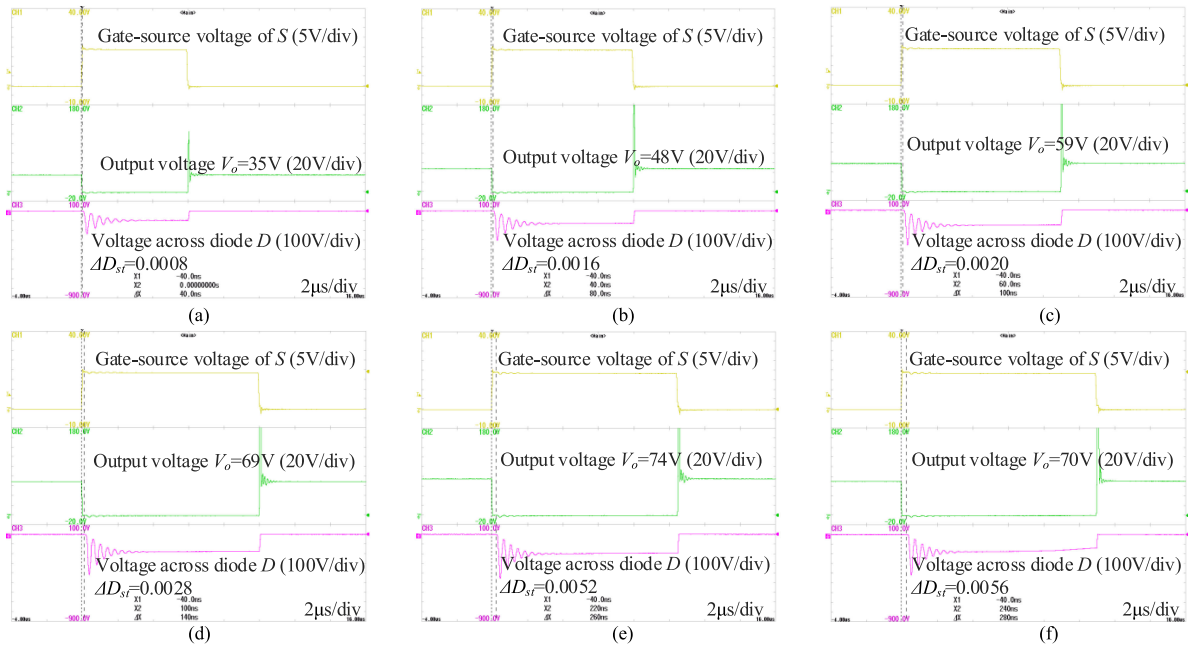


Fig. 15. Experimental results of Trans-Z-source with $N_1:N_2 = 36:12$. (a) $D_{st} = 0.12$. (b) $D_{st} = 0.16$. (c) $D_{st} = 0.18$. (d) $D_{st} = 0.20$. (e) $D_{st} = 0.21$. (f) $D_{st} = 0.22$.

Fig. 12, the mathematical derivations and analysis in Section IV part C can be verified.

B. Experimental Verification

The experimental prototype as shown in Fig. 13, is built in the laboratory to verify: first, the validity of the generalized equivalent circuit model for the three typical magnetically coupled impedance-source networks: Trans-Z-source, Γ -source,

and Y-source networks with parasitic resistances consideration, second, the corresponding mathematical derivations of the effects of parasitic resistances on the voltage gain under three different scenarios: resistance ratio, shoot-through duty ratio, and winding ratio, and third, the maximum voltage gain under the consideration of the three resistance ratios simultaneously. The experimental prototype of the magnetically coupled impedance-source converters as shown in Fig. 13 is controlled by FPGA Altera Cyclone 5CSEMA5F31C6N, where the shoot-through

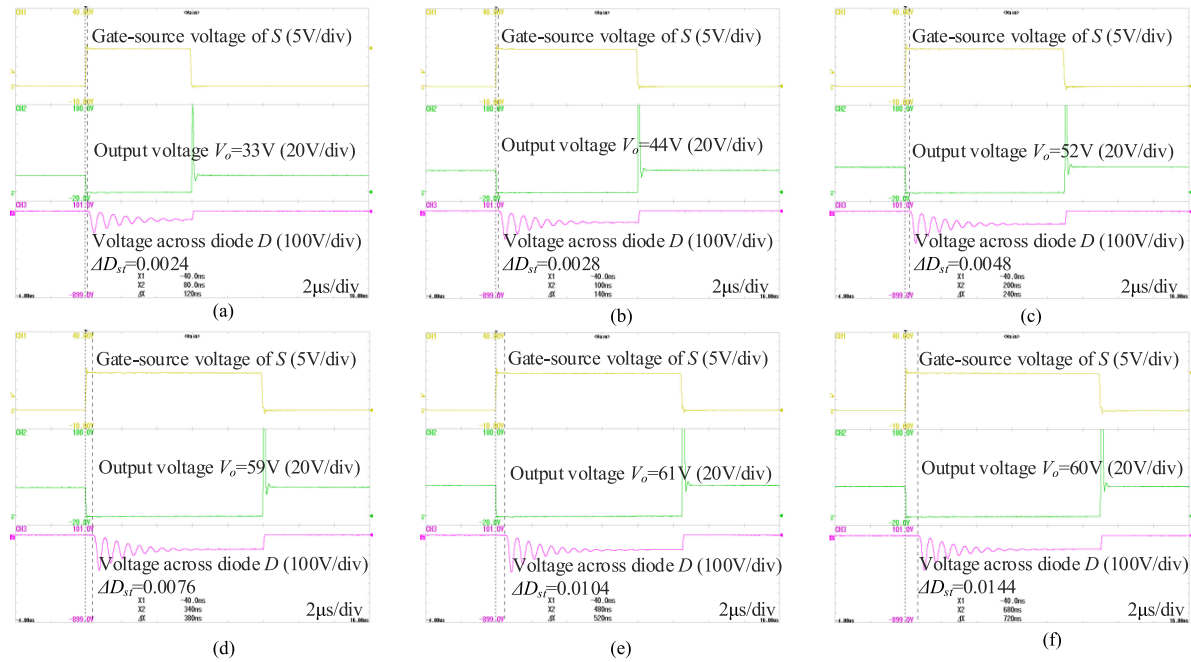


Fig. 16. Experimental results of Γ -source with $N_1:N_2 = 36:48$. (a) $D_{st} = 0.12$. (b) $D_{st} = 0.16$. (c) $D_{st} = 0.18$. (d) $D_{st} = 0.20$. (e) $D_{st} = 0.21$. (f) $D_{st} = 0.22$.

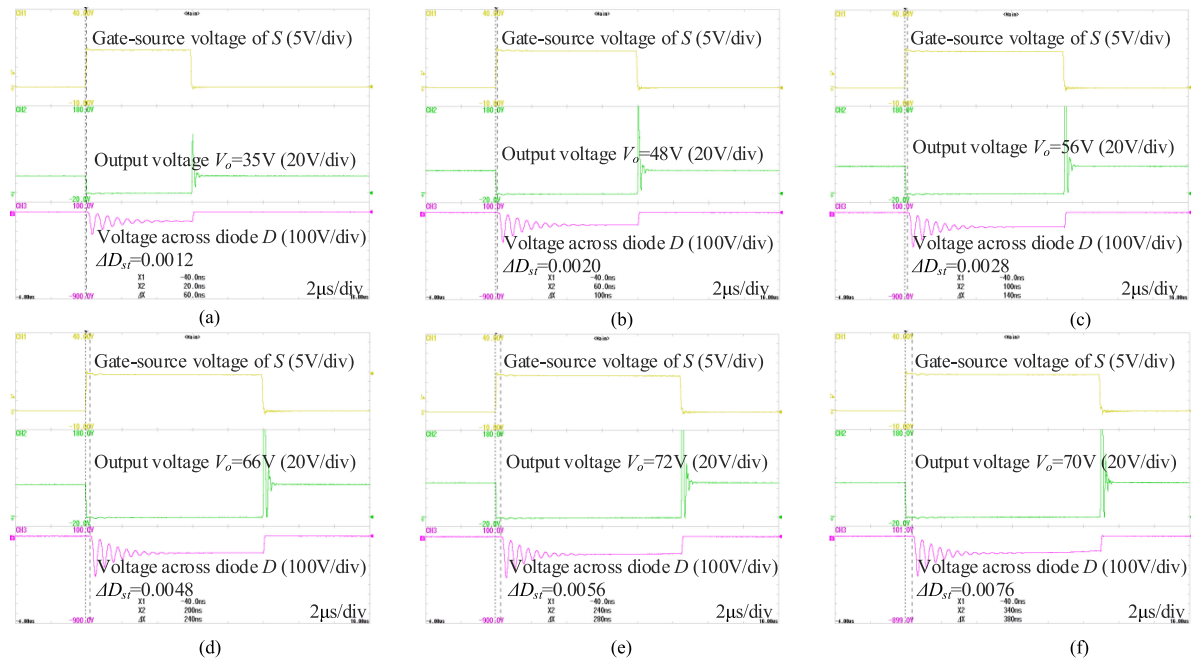


Fig. 17. Experimental results of Y -source with $N_1:N_2:N_3 = 30:6:18$. (a) $D_{st} = 0.12$. (b) $D_{st} = 0.16$. (c) $D_{st} = 0.18$. (d) $D_{st} = 0.20$. (e) $D_{st} = 0.21$. (f) $D_{st} = 0.22$.

duty ratio D_{st} is generated. The multiple stranded copper wire is used as the coils, the strand number is 100 and the diameter of each strand is designed as 0.1 mm, which is smaller than the skin depth 0.46 mm to reduce the skin effect, current rating is also designed to apply for all the experimental conditions. The ferrite core EE55B is used in this article, and core gaps are designed by considering about the magnetic permeability and saturation. The detailed experimental parameters of windings, capacitor,

switching devices, and other experimental environments are shown in Table III.

First, the experimental studies of Trans-Z-source are carried out. When $N_1:N_2 = 36:18$, $K = 2$ can be obtained according to (2), and Fig. 14 shows the experimental results, in which D_{st} changes from 0.2 to 0.31 gradually. Similarly, when $N_1:N_2 = 36:12$, $K = 3$, and Fig. 15 shows the experimental results, in which D_{st} changes from 0.12 to 0.22 gradually.

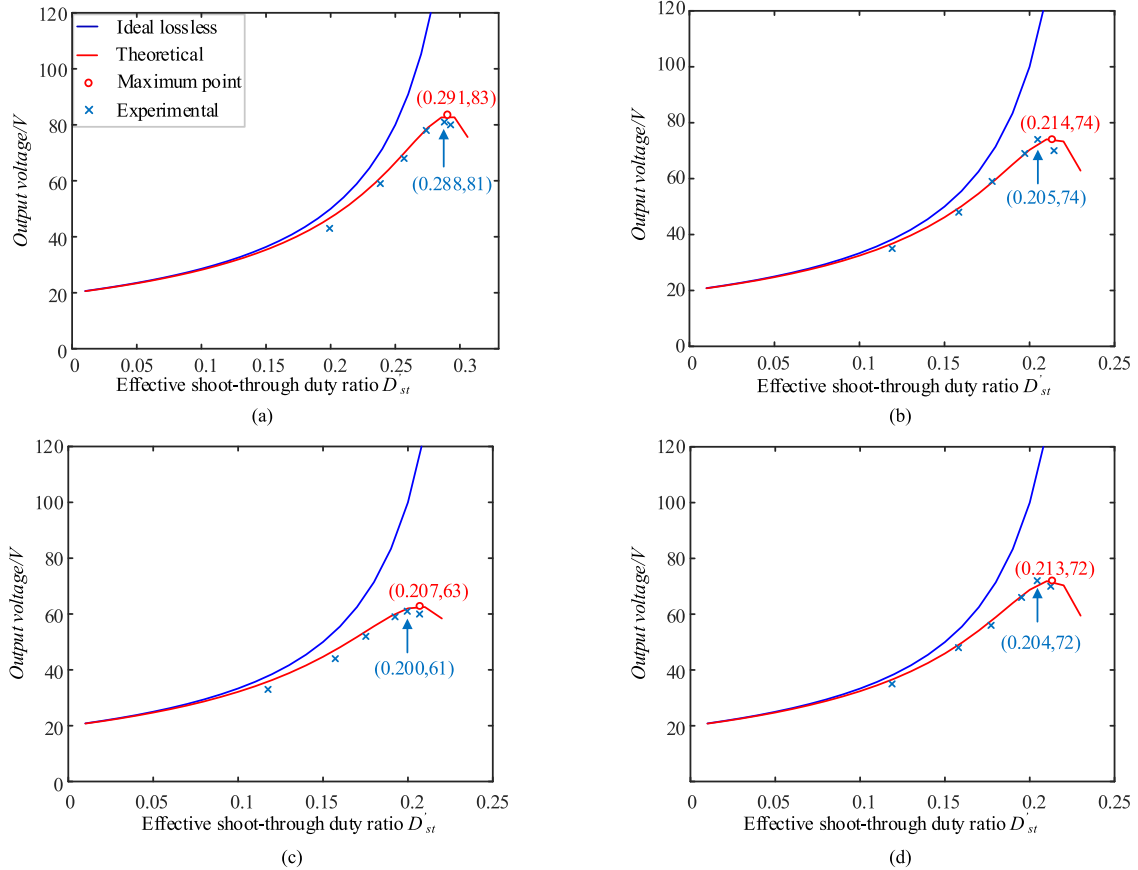


Fig. 18. Comparison of idea lossless, theoretical and experimental results. (a) Trans-Z-source with $N_1:N_2 = 36:18$. (b) Trans-Z-source with $N_1:N_2 = 36:12$. (c) Γ -source with $N_1:N_2 = 36:48$. (d) Y-source with $N_1:N_2:N_3 = 30:6:18$.

Second, the experimental studies of Γ -source with $N_1:N_2 = 36:48$ are carried out, $K = 3$ can be obtained according to (3), and Fig. 16 shows the experimental results, in which D_{st} changes from 0.12 to 0.22 gradually.

Third, the experimental studies of Y-source with $N_1:N_2:N_3 = 30:6:18$ are carried out, $K = 3$ can be obtained according to (4), and Fig. 17 shows the experimental results, in which D_{st} changes from 0.12 to 0.22 gradually.

Since the output voltage is affected by leakage inductances and parasitic resistances together, the effect of leakage inductances will lead to the reduction of effective shoot-through duty ratio ΔD_{st} , which can be calculated by comparing the output voltage with the voltage across the diode. Under the consideration of the leakage inductance, the real effective shoot-through duty ratio becomes $D'_{st} = D_{st} - \Delta D_{st}$ [17]. The gate-source voltage, output voltage and voltage across the diode of different magnetically coupled impedance-source network topologies are shown in Figs. 14–17, the output voltage curves versus with D'_{st} are shown in Fig. 18.

1) *Verification of Generalized Equivalent Circuit Model:* All the experimental results in Fig. 18 are consistent with the theoretical curves derived by the generalized equivalent circuit model proposed in this article, which means that the generalized equivalent circuit model can represent the Trans-Z-source, Γ -source, and Y-source networks, thus the validity of the generalized equivalent circuit model is verified.

2) *Resistance Ratio, Shoot-Through Duty Ratio, and Winding ratio:* In practical case, unlike the simulation part, both α , β , and γ exist, so the effect of resistance ratio, shoot-through duty ratio and winding ratio on the voltage gain is not able to be verified individually and separately when only α , β or γ is considered. However, Fig. 18 shows the experimental results under different resistance ratios, different shoot-through ratios, different winding ratios, and they are all consistent with the theoretical curves derived by the equivalent circuit model, thus the effects of parasitic resistances on the voltage gain under three different scenarios: first, resistance ratio, second, shoot-through duty ratio, and third, winding ratio can be verified too.

3) *Maximum Voltage Gain Under Ratios α , β , and γ Consideration:* As shown in Fig. 18, the experimental maximum points are basically consistent with the theoretical values derived by (49), thus the deduced maximum voltage gain (49) under ratios α , β , and γ consideration is also verified.

VI. CONCLUSION

Magnetically coupled impedance-source networks are proposed to achieve a higher voltage gain with smaller shoot-through duty ratio. However, the voltage gain of the impedance-source converter is seriously affected by the parasitic resistances, which should be studied and investigated. In this article, the generalized equivalent circuit models under parasitic resistances

consideration is first proposed for the three typical magnetically coupled impedance-source networks, namely Trans-Z-source, Γ -source, and Y-source. Based on the proposed equivalent circuit models, the voltage gain under parasitic resistances condition can be derived and discussed in details under three different conditions: different resistance ratio, different shoot-through duty ratio, and different winding ratio, and the maximum voltage gain under the consideration of the three resistance ratios simultaneously is also derived. Finally, simulation and experimental results are provided to verify the proposed equivalent circuit models, the deduced corresponding mathematical equations and the discussed characteristics in this article.

REFERENCES

- [1] Y. P. Siwakoti, F. Z. Peng, F. Blaabjerg, P. C. Loh, and G. E. Town, "Impedance-source networks for electric power conversion part I: A topological review," *IEEE Trans. Power Electron.*, vol. 30, no. 2, pp. 699–716, Feb. 2015.
- [2] F. Z. Peng, "Z-source inverter," in *Proc. IEEE-IAS Annu. Meeting*, 2002, pp. 775–781.
- [3] F. Z. Peng, "Z-source inverter," *IEEE Trans. Ind Appl.*, vol. 39, no. 2, pp. 504–510, Mar./Apr. 2003.
- [4] M. Zhu, K. Yu, and F. L. Luo, "Switched inductor Z-source inverter," *IEEE Trans. Power Electron.*, vol. 25, no. 8, pp. 2150–2158, Aug. 2010.
- [5] J. Anderson and F. Z. Peng, "Four quasi-Z-source inverters," in *Proc. IEEE Power Electron. Specialists Conf.*, Jun. 2008, pp. 2743–2749.
- [6] F. Z. Peng, M. S. Shen, and Z. M. Qian, "Maximum boost control of the Z-source inverter," *IEEE Trans. Power Electron.*, vol. 20, no. 4, pp. 833–838, Jul. 2005.
- [7] P. C. Loh and F. Blaabjerg, "Magnetically coupled impedance-source inverters," *IEEE Trans. Ind Appl.*, vol. 49, no. 5, pp. 2177–2187, Sep./Oct. 2013.
- [8] W. Qian, F. Z. Peng, and H. Cha, "Trans-Z-source inverters," *IEEE Trans. Power Electron.*, vol. 26, no. 12, pp. 3453–3463, Dec. 2011.
- [9] P. C. Loh, D. Li, and F. Blaabjerg, " Γ -Z-source inverters," *IEEE Trans. Power Electron.*, vol. 28, no. 11, pp. 4880–4884, Nov. 2013.
- [10] Y. P. Siwakoti, P. C. Loh, F. Blaabjerg, and G. E. Town, "Y-source impedance network," *IEEE Trans. Power Electron.*, vol. 29, no. 7, pp. 3250–3254, Jul. 2014.
- [11] M. Nguyen, Y. Lim, and S. Park, "Improved trans-Z-source inverter with continuous input current and boost inversion capability," *IEEE Trans. Power Electron.*, vol. 28, no. 10, pp. 4500–4510, Oct. 2013.
- [12] Y. P. Siwakoti, F. Blaabjerg, and P. C. Loh, "Quasi-Y-source boost DC–DC converter," *IEEE Trans. Power Electron.*, vol. 30, no. 12, pp. 6514–6519, Dec. 2015.
- [13] Y. P. Siwakoti, P. C. Loh, F. Blaabjerg, S. J. Andreasen, and G. E. Town, "Y-source boost DC/DC converter for distributed generation," *IEEE Trans. Ind. Electron.*, vol. 62, no. 2, pp. 1059–1069, Feb. 2015.
- [14] Y. P. Siwakoti, F. Blaabjerg, V. P. Galigekere, A. Ayachit, and M. K. Kazmierczuk, "A-source impedance network," *IEEE Trans. Power Electron.*, vol. 31, no. 12, pp. 8081–8087, Dec. 2016.
- [15] A. Hakemi, M. Sanatkar-Chayjani, and M. Monfared, " Δ -source impedance network," *IEEE Trans. Ind. Electron.*, vol. 64, no. 10, pp. 7842–7851, Oct. 2017.
- [16] Y. Wang *et al.*, "A family of Y-source DC/DC converter based on switched inductor," *IEEE Trans. Ind Appl.*, vol. 55, no. 2, pp. 1587–1597, Mar./Apr. 2019.
- [17] Y. P. Siwakoti, P. C. Loh, F. Blaabjerg, and G. E. Town, "Effects of leakage inductances on magnetically coupled Y-source network," *IEEE Trans. Power Electron.*, vol. 29, no. 11, pp. 5662–5666, Nov. 2014.
- [18] H. Liu *et al.*, "A family of high step-up coupled-inductor impedance-source inverters with reduced switching spikes," *IEEE Trans. Power Electron.*, vol. 33, no. 11, pp. 9116–9121, Nov. 2018.
- [19] H. Liu *et al.*, "High step-up Y-source inverter with reduced DC-link voltage spikes," *IEEE Trans. Power Electron.*, vol. 34, no. 6, pp. 5487–5499, Jun. 2019.
- [20] Y. P. Siwakoti, F. Blaabjerg, and P. C. Loh, "New magnetically coupled impedance (Z-) source networks," *IEEE Trans. Power Electron.*, vol. 31, no. 11, pp. 7419–7435, Nov. 2016.



Xiangfei Kong (Student member, IEEE) was born in Liaoning Province, China. He received the B.Eng. and M.Eng. degrees in electrical engineering from the China University of Petroleum, Shandong, China, in 2013 and 2018, respectively. He is currently working toward the Ph.D. degree in electrical and computer engineering with the University of Macau, Macau, China.

He was an Electrical Engineer with Liaohu Oil-field, China National Petroleum Corporation, Liaoning, China, from 2013 to 2014. He was a Research Assistant with the Shenyang Institute of Automation, Chinese Academy of Sciences, Liaoning, China, in 2018. His research interests include power electronics and control systems.



Chi-Kong Wong (Member, IEEE) received the B.Sc. and M.Sc. degrees in electrical and electronics engineering from the University of Macau (UM), Macao, China, in 1993 and 1997, respectively, and the Ph.D. degree in electrical engineering from Tsinghua University, Beijing, China, in 2007.

Since 1993, he has been a Teaching Assistant with the Faculty of Science and Technology, UM, where he was promoted as a Lecturer and an Assistant Professor in 1997 and 2008, respectively. His current research interests include power electronics controllers, power system analysis, power quality compensators, and renewable energy.

Dr. Wong has been an IEEE Student Branch Officer since 1997. He is currently the Vice-Chair of IEEE Macau Section and the Committee Member of IEEE Macau PES/PELS Joint Chapter.



Chi-Seng Lam (Senior member, IEEE) received the Ph.D. degree in electrical and electronics engineering from the University of Macau (UM), Macao, China, in 2012. He completed the Clare Hall Study Programme in the University of Cambridge, Cambridge, U.K., in 2019.

From 2006 to 2009, he was an Electrical and Mechanical Engineer with UM. From 2009 to 2012, he simultaneously worked as a Laboratory Technician with UM and worked toward his Ph.D. degree. In 2013, he was a Postdoctoral Fellow with the Hong Kong Polytechnic University, Hong Kong, China. He is currently an Associate Professor with the State Key Laboratory of Analog and Mixed-Signal VLSI and Institute of Microelectronics, UM, and also with the Department of Electrical and Computer Engineering, Faculty of Science and Technology, UM. He has coauthored or coedited four books: *Design and Control of Hybrid Active Power Filters* (Springer, 2014), *Parallel Power Electronics Filters in Three-phase Four-wire Systems—Principle, Control, and Design* (Springer, 2016), *Tutorials in Circuits and Systems Selected Topics in Power, RF, and Mixed-Signal ICs* (River Publishers, 2017), and *Adaptive Hybrid Active Power Filters* (Springer, 2019), and more than 100 technical journals and conference papers. He holds four U.S. patents and two Chinese patents. His research interests include power quality compensators, renewable energy generation, integrated power electronics controllers, power management integrated circuits, and wireless power transfer.

Dr. Lam was a member of Organizing Committee or Technical Program Committee of several IEEE international conferences, including Annual Conference of the IEEE Industrial Electronics 2019, Asian Solid-State Circuits Conference 2019, Asia-Pacific Power and Energy Engineering Conference 2019, Annual Conference of the IEEE Industrial Electronics 2018, International Conference on Industrial Electronics for Sustainable Energy Systems 2018, Asia and South Pacific-Design Automation Conference 2016, and Region 10 Conference 2015. He was a tutorial speaker of Asia-Pacific Power and Energy Engineering Conference 2019. He was a recipient or corecipient of the IEEE Power and Energy Society Chapter Outstanding Engineer Award in 2016, Best Track Paper Award of Asia-Pacific Power and Energy Engineering Conference in 2019, Best Paper Award of International Conference on Integrated Circuits, Technologies and Applications in 2019, Merit Paper Award of 3rd Regional Inter-University Postgraduate Electrical and Electronic Engineering Conference in 2005, the Macao Science and Technology Invention Award (2nd Class and 3rd Class), and the Research and Development Award for Postgraduates (Ph.D.) in 2018, 2014, and 2012, respectively. He was the Chair of IEEE Macau CAS Chapter from 2017 to 2018. He is currently the Vice-Chair of IEEE Macau Section and the Chair of IEEE Macau IES Chapter.